A THESIS FOR THE DEGREE OF MASTER OF SCIENCE

Crystal Structures and Reaction Mechanism of 1-Cys Peroxiredoxin from *Vibrio vulnificus*

패혈증 비브리오균 Prx3 의 구조적 특성과 작용기전 규명

August, 2016

Jin Sook Ahn

Department of Agricultural Biotechnology
College of Agriculture and Life Sciences
Seoul National University

석사학위논문

Crystal Structures and Reaction Mechanism of 1-Cys Peroxiredoxin from *Vibrio vulnificus*

지도교수 하 남 출

이 논문을 석사학위논문으로 제출함

2016 년 8 월

서울대학교 대학원

농생명공학부

안 진 숙

안진숙의 석사학위논문을 인준함

2016 년 8 월

위원장 서진호 (인)

부위원장 하남출 (인)

위원 최상호 (인)

ABSTRACT

Vibrio vulnificus is capable of causing severe food-borne and often fatal wound infections. It causes two distinct disease syndromes, life-threatening septicemia and necrotizing wound infections. Under reactive oxygen species (ROS) and reactive nitrogen species (RNS) stress, pathogens have evolved elaborate strategies to survival against to host defense systems. Peroxiredoxins (Prxs) are the ubiquitous cysteine-based peroxidase enzymes. Recently, a new type of Prx, called *Vv*Prx3, was identified in *V. vulnificus* as an essential gene for survival of the bacterium in a mouse model. It belongs to 1-Cys Prx family proteins that contain only one catalytic cysteine residue. Interestingly, *Vv*Prx3 was induced by the transcriptional factor, IscR, different from other types of Prx in *V. vulnificus*. In this study, I determine the crystal structures of *Vv*Prx3 from *V. vulnificus* both in the reduced and the oxidized forms at high resolutions. The crystal structure in the reduced form showed a typical dimeric interface, previously characterized as 'A-type interface'. The oxidized structure revealed a novel oligomeric interface, which is mediated by a disulfide bond between the catalytic cysteine residues. Ensuing biochemical studies showed that this disulfide was induced by treatment of peroxides and NO. The oligomeric state of Prx3, which was shown in the crystal structure, was confirmed by analytic size exclusion chromatography. I also found that a reductase Grx3 can efficiently reduce the intermolecular disulfide of *Vv*Prx3. Taken together, I propose a novel function of 1-Cys peroxiredoxin in direct scavenging of peroxides and NO stresses via a novel type

of oligomerization, and these findings would help understand diverse functions of peroxiredoxins during pathogenic process at the molecular level. It may further contribute to development of drugs or food sanitizers to cope with the food-borne diseases caused by *Vibrio vulnificus* by controlling the Prx3 functions based on the structure of Prx3.

Keywords: ***Vibrio vulnificus*****, 1-Cys Prx, hydrogen peroxide, nitric oxide**
Student Number: **2014-22933**

CONTENTS

LIST OF FIGURES

LIST OF TABLE

I. INTRODUCTION

Vibrio vulnificus is Gram negative, curved and rop-shape bacterium found in coastal marine and estuarine environments. *V. vulnificus* is the causative agent of food-borne diseases such as life-threatening septicemia and especially it is lethal to immune compromised persons (Beckman et al., 1990). When the pathogens infect host cells, the host macrophages produce large amounts of nitric oxide (NO), superoxide anion, and hydrogen peroxide (H_2O_2) to prevent bacterial infections (Murray and Nathan, 1999). Reactive oxygen species (ROS) and reactive nitrogen species (RNS) can interact with numerous targets in a microbial cell, including thiols, metal centres, protein tyrosines, nucleotide bases and lipids (Cabiscol et al., 2000). To protect against ROS and RNS stress from host immune system, *V. vulnificus* have evolved efficient defense systems that rapidly detoxify potentially-damaging ROS, such as peroxides and superoxide anion (Wood et al., 2003a).

Peroxiredoxins (Prxs) represent a superfamily of thiol-dependent peroxidases that can reduce and decompose peroxides, such as H_2O_2 and alkyl hydroperoxides, and peroxynitrite (Huaxia et al., 2015). Prxs are ubiquitously found from human to bacteria, and highly conserved throughout evolution. They play a crucial role in detoxification of peroxides in the cytosol. Prxs have a peroxidatic Cys (C_P) that reacts with peroxides in the N-terminal core domain. The catalytic cycle of peroxiredoxin can be divided into three possible redox states: (i) peroxidation, (ii) resolution, and (iii) recycling (Pedrajas et al., 2015). In the peroxidation step, the C_P is oxidized to

cysteine-sulfenic acid (C_P-SOH) by attacking the O-O bond of peroxides, resulting in decomposition of the toxic peroxides (Rhee et al., 2007). In the resolution step, oxidized catalytic cysteine condenses with the resolving cysteine, another protein, or small molecule (1-Cys mechanism) to form a disulfide. Finally, in the recycling step, the disulfide bond is reduced by cellular reduction systems, regenerating the free thiols (Knoops et al., 2011).

Depending on the resolution step, Prxs are classified into three types, referred to as typical 2-Cys, atypical 2-Cys, and 1-Cys Prxs (Hall et al., 2011). Both typical and atypical 2-Cys Prxs have additional conserved cysteine residue, called resolving cysteine (C_R), which forms a stable disulfide bond with the C_P-SOH. While the C_R is from another subunit in typical 2-Cys Prxs, it is located within the same subunit in atypical 2-Cys Prxs (Lee et al., 2015). The disulfide bond can be returned to two free thiols converted by thioredoxin (Trx) and alkyl hydroperoxidase subunit F (AphF) in 2-Cys Prxs (Li et al., 2005). It has been implicated that the C_P-SOH in 1-Cys Prxs is reduced without the disulfide within Prxs by external reductants such as glutaredoxin (Grx) and/or the reduced form of glutathione (GSH) (Jeong et al., 2000).

The structures of Prxs have been extensively characterized since the first Prx structure of the human PrxVI (Declercq et al., 2001). All Prxs exhibit highly conserved Prx-folds that consist of an N-terminal Trx-fold region containing the C_P residue and peripheral secondary structural elements. Although the oligomeric states of Prxs differ depending on the types of Prxs, all oligomeric Prxs are formed via two distinct interfaces; B-type or A-type interface. The central β-sheets of the Trx core

are involved in the B-type interface, while a short α-helical regions are packed each other in the A-type interface (Karplus and Hall, 2007). In typical 2-Cys Prxs, the dimers are primarily formed via the B-type interface, in which the C_P and C_R are located in different protomers a short distance and the disulfide formation is facilitated by peroxides (Parsonage et al., 2005). For most 2-Cys Prxs, five dimers are further associated via the A-type interface to form a doughnut-like decamer (Wood et al., 2002). Redox-dependent structural changes in the C_P-containing loop and decamer formation have been reported in some typical 2-Cys Prxs (Hirotsu et al., 1999). When in the reduced or overoxidized states (C_P-SO_2H or C_P-SO_3H in C_P residue), the C_P-containing loop exhibits a "fully-folded" conformation that highly favors decamer formation (Karplus and Hall, 2007). However, Prxs form a mixture of low-order oligomeric assemblies in the oxidized state (referred to as disulfide state in this study) harboring a disulfide bond between the C_P and C_R with "locally-unfolded" conformation in the C_P-containing loop (Randall et al., 2016). In contrast, most atypical 2-Cys Prxs and 1-Cys Prxs exhibit a dimeric assembly via the A-type interface (Evrard et al., 2004). Bacterial 1-Cys Prxs do not have a C-terminal extension region that contains the C_R in typical 2-Cys Prxs (Li et al., 2005).

Vibrio vulnificus has three different kinds of Prxs: Prx1, Prx2, and Prx3. Prx1 and Prx2 belong to typical 2-Cys Prx family proteins, and their expressions are controlled by H_2O_2 -activated transcription factor OxyR (Jo et al., 2015). *V. vulnificus* Prx3 (*Vv*Prx3) is a 1-Cys Prx with one conserved catalytic cysteine (Cys48), and it has been shown to play an essential role in pathogenicity in a mouse model (Lim

et al., 2014). Expression of *Vv*Prx3 is controlled by IscR, which is activated by the lack of the Fe-S cluster or by NO treatment (Hyduke et al., 2007). In this study, I determine the crystal structures of *Vv*Prx3 in two different forms and in complex with H_2O_2. Based on the crystal structures, I present a molecular mechanism of 1-Cys Prxs describing a new type of dimeric interface with the new function of scavenging nitric oxide (NO).

II. MATERIALS AND METHODS

2.1. Plasmid construction

The *Vv*Prx3 (C48D/C73S) and *Vv*PRX3 (C73S) genes of *V. vulnificus* was amplified by polymerase chain reaction (PCR) using the following two primers (forward: 5'- GGTCATATGATCGCTCAAGGCCAAACTTTACC -3'; reverse: 5'-CCTCTCGAGCGCGGCAAGAATCGTTTCAGC-3'). The underlined sequences represent the NdeI and XhoI restriction sites, respectively. The amplified product and the expression vector pET-21C (Invitrogen) were digested with NdeI and XhoI restriction enzymes. The digested product was inserted into the expression vector pET-21C by DNA ligase. The ligation mixture was transformed into *Escherichia coli* C43 (DE3) competent cell by heat-shock. Finally, the recombinant plasmid was confirmed by DNA sequencing.

2.2. Site direct mutagenesis

A single mutation of cysteine to serine was performed using the Quick Change XL Site-directed Mutagenesis Kit. The complementary mutagenic primers were used to two subsequent PCR reactions for the expression of *Vv*Prx3 (C48D/C73S) (Ho et al., 1989). After amplification, the PCR mixture was incubated with DpnI at 37°C for 2

hours. For overexpression of the recombinant DNA, the mutant plasmid was transformed into the *E. coli* C43 (DE3) competent cell by heat-shock. The sequence of mutant plasmid was confirmed by automated DNA sequencing.

2.3. Purification of Prx3 (C48D/C73S) and Prx3 (C73S) proteins

2.3.1. Overexpression

To expression of the recombinant proteins, a single colony from the *E.coli* C43 (Prx3 C73S or C48DC73S) was inoculated into 25 mL LB broth including 50 μg/mL ampicillin (Duchefa, Netherlands) and incubated it at 37°C for 12 hours. The resultant seed culture was inoculated to 1.5 L of LB medium containing 50 μg/mL ampicillin. The cell were grown at 37°C until an OD 600 of 0.5 was attained and then induced with 0.5 mM isopropyl-β-D-thiogalacto pyranoside (IPTG) for 6 h at 30°C. The cells were harvested by centrifugation at 3850 g for 10 min and resuspended with lysis buffer containing 20 mM Tris-HCl (pH 8.0), 0.15 M NaCl, and 2 mM 2-mercaptoethanol. Cell disruption was done by French press (Beijer, Sweden) at 20 kpsi. After disrupting the cells by French press, the crude lysate was centrifuged at 10000 g for 30 min and cell debris was discarded.

2.3.2. Affinity chromatography

The purification was conducted in three steps. The supernatant was applied to Ni^{2+}–NTA affinity resin that had been pre-incubated with lysis buffer. This mixture was then stirred for 1 h at 4°C. After the mixture was stirred on the column, the non-bound fraction was washed off with lysis buffer supplemented with 20 mM imidazole. The target protein was eluted with 25 mL of lysis buffer supplemented with 250 mM imidazole. The eluted fractions containing Prx3 were collected, and then the hexa-histidine tag was cleaved with recombinant TEV protease by incubation at room temperature for 6 hours (Jiao et al., 2013).

2.3.3. Ion-exchange chromatography

The eluted recombinant proteins were diluted by the buffer (20 mM Tris-HCl pH 8.0, 2 mM 2-mercaptoethanol) at 1:4 ratio. The diluted protein sample was loaded to ion exchange chromatography on Hitrap Q column (GE Healthcare, USA).The protein was eluted from the column with a linear gradient of 0–1 M NaCl in lysis buffer.

2.3.4. Size exclusion chromatography

As a final purification step, gel filtration was performed using HiLoad Superdex 200 columns (GE Healthcare, USA) pre-equilibrated with 20 mM Tris-HCl (pH 8.0)

buffer containing 150 mM NaCl and 2 mM 2-mercaptoethanol. The purified proteins were concentrated more than 20 mg/ml using Vivaspin 20 (Sartorius, Germany).

2.4. Crystallization

Initial crystallization screen of *Vv*Prx3 (C48D/C73S) and *Vv*Prx3 (C73S) were performed by the sitting-drop vapor-diffusion method using commercial screening solution from Documents Hampton Research and Anatrace. The sitting drops were mixed with 200 nL drops consisting of a 1:1 ratio of protein and reservoir solutions by using mosquito robot (TTP Labtech, United Kingdom). The crystals of *Vv*Prx3 (C48D/C73S) were obtained in the precipitant solution containing 0.8 M sodium citrate, and 0.1 M Tris-HCl (pH 6.5). To improve the quality of the crystals, two components of initial condition were optimized by varying the salt concentration and the pH of precipitant solutions. Crystals of *Vv*Prx3 (C73S) appeared in 5 days in the precipitant solution containing 0.1 M sodium citrate (pH 5.5), 0.2 M ammonium acetate, 22% (wt/vol) PEG 4000. To obtain *Vv*Prx3 (C48D/C73S)-H_2O_2 complex crystals, the crystals were soaked in precipitant solution supplemented with H_2O_2.

2.5. Structure determination and refinement

Crystals were soaked into appropriate mother liquor supplemented with 20% glycerol, mounted on cryo-loops and flash-cooled in liquid nitrogen stream at −173°C.

X-ray diffraction datasets were collected with the Pohang Accelerator Laboratory Beam Line 5C and processed with the HKL2000 package (Otwinowski and Minor, 1997). The structure of *Vv*Prx3 (C48D/C73S) was solved by the molecular replacement method with the program MOLREP in the CCP4 package (Winn et al., 2011) using a putative thioredoxin reductase from *Burkholderia cenocepacia* (PDB code 4F82) as a search model. The final structure of *Vv*Prx3 (C48D/C73S) was refined at 1.9 Å resolution using the PHENIX program (Afonine et al., 2012) .The crystal of *Vv*Prx3 (C48D/C73S) belongs to the $P3_221$ space group, with unit cell dimensions of a =75.08 Å, b = 97.72 Å and c = 97.49 Å (Table 1). The initial model of *Vv*Prx3 (C73S) and H_2O_2 binding complex structure were determined by molecular replacement using the structure of *Vv*Prx3 (C48D/C73S) and refined at a 1.5 Å resolution (Table 1). The crystals belong to the space group $P2_12_12_1$, with a =39.5 Å, b = 57.4 Å and c = 124.4 Å, and two protein molecules in the asymmetric unit. X-ray diffraction data of *Vv*Prx3 (C48D/C73S) with H_2O_2 were collected at 1.9 Å resolution and the structure was built using the Coot (Emsley et al., 2010). Some statistics of data collection and processing are presented in Table 1.

2.6. Oxidation of VvPrx3 by H_2O_2 or NO

To prepare the reduced *Vv*Prx3 (C73S) protein, 20 mM 1,4-Dithiothreitol (DTT; Sigma, USA) was added to purified *Vv*Prx3 (C73S) protein, and then removed by Hitrep 26/10 desalting column (GE Healthcare, USA) placed in 20 mM Tris buffer

(pH 8.0) containing 150 mM NaCl. The reduced *Vv*Prx3 (C73S) mutant protein (55 nmole) was reacted with given concentrations of H_2O_2 or t-BOOH for 30 min at 25˚C in 1 ml of 20 mM Tris buffer (pH 8.0) containing 150 mM NaCl. The reaction mixture was treated with iodoacetamide (IAA) to stop the reaction and then subjected to SDS-PAGE under non-reducing or reducing conditions. To react with NO, reduced *Vv*Prx3 (C73S) protein (10 nmole) was treated with 1 mg of NO/PPNPs in 10 ml reaction mixture in 20 mM Tris (pH 7.5) and 150 mM NaCl. The amount of NO was calculated based on 3.3 nmole NO released per hour in 1 mg NO/PPNPs (Nurhasni et al., 2015).

2.7. Analytic size exclusion chromatography

A Superose 6 HR 10/30 column coupled to an FPLC instrument (GE Healthcare, USA) was equilibrated with 20 mM Tris (pH 8.0) and 150 mM NaCl. Samples were incubated with 10 µM H_2O_2 for 30 min at room temperature before loading onto the column to form intermolecular disulfide bond of *Vv*Prx3 (C73S). Samples were loaded for chromatography, which was performed at a flow rate of 0.2 ml/min. Several standard preparations were run to calibrate the column (Fig. 1). Absorbance at 280 nm after elution was monitored.

2.8. Reductase activity of Grx3 on the disulfided VvPrx3 protein

Samples containing approximately 30 μM *Vv*Prx3 (C73S) were incubated with 10 μM H_2O_2 for making intermolecular disulfide bridges between C_P's. Highly 15 μM of purified Grx3 and GSH (Sigma, USA). The reaction was initiated by the addition of 15 μM of Grx3 and GSH. At the indicated times, the reaction was immediately stopped by adding 2.5 mM IAA, and the mixture was separated on 15% SDS-PAGE gel.

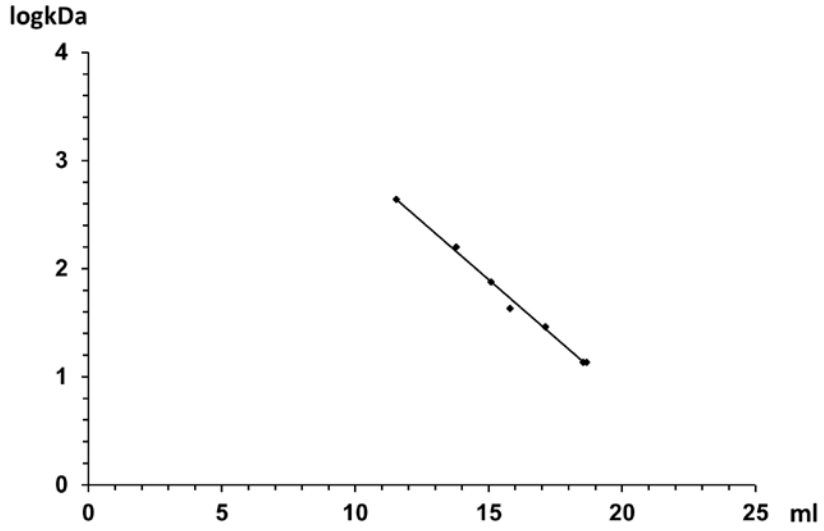

Figure 1. A standard curve of analytic size exclusion chromatography. 11.54 ml : ferritin (440 kDa), 13.79 ml : Aldolase (158 kDa), 15.09 ml : Conalbumin (75 kDa), 15.8 ml : Ovalbumin (43 kDa), 17.12 ml : carbonic anhydrase (29 kDa), 18.54 ml : Ribonuclease A (13.7 kDa), 18.66 ml : Ribonuclease A (13.7 kDa).

III. RESULTS

3.1. Overexpression and purification of Prx3 (C48D/C73S) and Prx3 (C73S) proteins

*Vv*Prx3 has two cysteine residues (Cys48 and Cys73), in which Cys48 is the C_P residue and Cys73 is functionally uncharacterized (Lim et al., 2014). To focus on the function of Cys48 and prevent unwanted modification at Cys73, Cys73 was replaced with a serine residue in this study. To overexpression of Prx3 (C48D/C73S) and Prx3 (C73S) proteins, recombinant plasmids were transformed into C43 (DE3) competent cells. The cloned Prx3 gene containing a C-terminal His_6-tagged was affinity purified from the solution. The target protein was bound onto a 5 ml HiTrap Q column and eluted with 270 mM NaCl. Then this sample was purified by gel-filtration using HiLoad 16/60 Superdex 200 column. The success of each step was monitored by SDS–PAGE (Fig. 2).

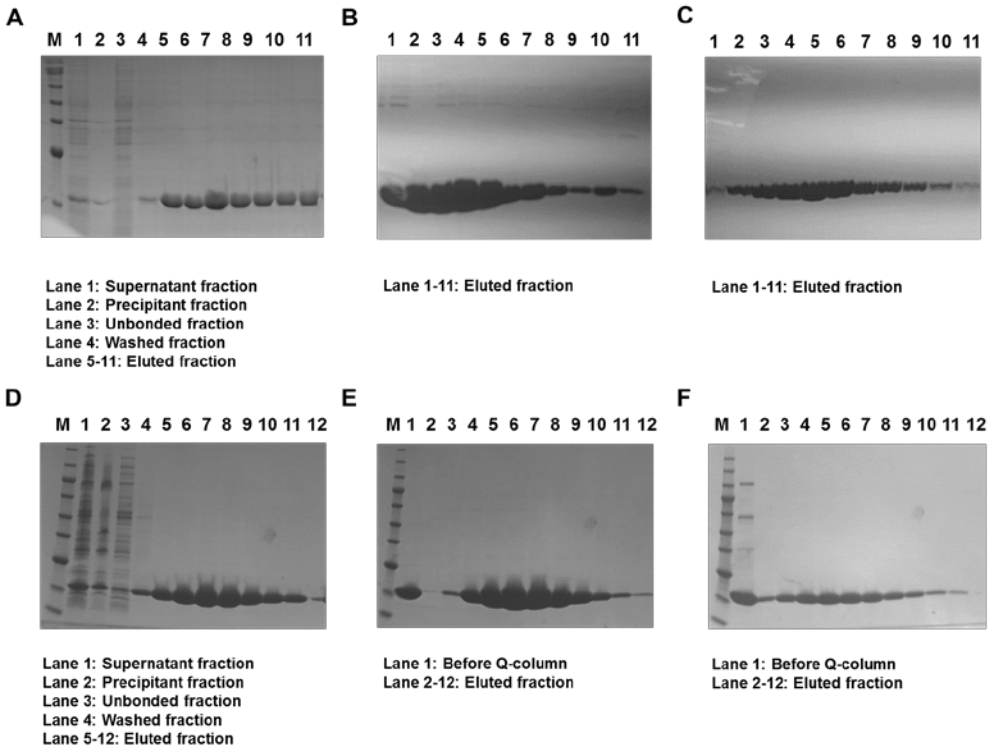

Figure 2. Purification profile from the Ni-NTA chromatography (C48D/C73S; A, C73S; D), the anion-exchange chromatography (C48D/C73S; B, C73S; E), and the size-exclusion chromatography (C48D/C73S; C, C73S; F).

3.2. Crystals of *Vv*Prx3 (C48D/C73S) and (C73S)

The purified Prx3 (C48D/C73S) and Prx3 (C73S) were concentrated up to 27 and 40 mg/ml for the crystallization. The crystals of Prx3 (C48D/C73S) were obtained in the precipitant solution containing 0.8 M sodium citrate, and 0.1 M Tris-HCl (pH 6.5). To improve the quality of the crystals, add 0.2 M NaCl in the initial crystal conditions of Prx3 (C48D/C73S) (Fig. 3A). The crystal condition of *Vv*Prx3 (C73S) crystals were 0.1 M sodium citrate tribasic dihydrate (pH 5.6), 0.2 M ammonium acetate, 30% (wt/vol) PEG 4000. The optimized condition for the *Vv*Prx3 (C73S) crystals were 0.1 M sodium citrate (pH 5.6), 0.2 M ammonium acetate, 22% (wt/vol) PEG 4000 (Fig. 3B). To obtain *Vv*Prx3 (C48D/C73S)-H_2O_2 complex crystals, a high concentration (500 µM) of H_2O_2 was incubated with crystals of *Vv*Prx3 (C48D/C73S). After 10 days, the H_2O_2-soaked *Vv*Prx3 (C48D/C73S) crystals were flash-frozen using the same cryoprotectant as *Vv*Prx3 (C48D/C73S) crystals in a nitrogen stream at −173°C.

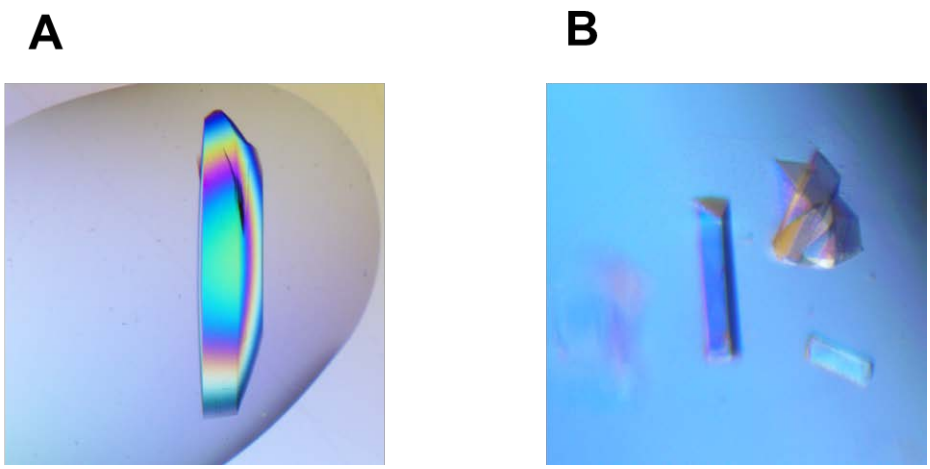

Figure 3. The crystals of Prx3 (C48D/C73S; A) and Prx3 (C73S; B).

3.3. Structural determination of *Vv*Prx3

I obtained the crystals of a *Vv*Prx3 (C48D/C73S) variant, where the C_P Cys48 is replaced with aspartic acid to mimic overoxidized cysteine residues, as previously reported in a study of *P. aeruginosa* OxyR . The space group of *Vv*Prx3 (C48D/C73S) crystal belongs to $P3_221$, and its structure was determined by the molecular replacement approach. This structure of the *Vv*Prx3 (C48D/C73S) variant is referred to as the reduced (or overoxidized) *Vv*Prx3 structure in this study. The final model was refined at 1.9 Å (R factor = 0.213, R_{free} = 0.258), and contains one protomer (residues 1-18, residues 22-157) in the asymmetric unit (Fig 4A; Table 1). The crystals of *Vv*Prx3 (C73S) gave a different space group, $P2_12_12_1$ and its structure was solved at 1.5 Å resolution by the molecular replacement method (Fig 4B). The resulting structure was refined to R factor of 0.181 and R_{free} of 0.198. The final model comprises residues 1-157, and contains two protein molecules in the asymmetric unit (Table 1).

The crystal structures of *Vv*Prx3 revealed that its protomer exhibits a compact and spherical structure without the C-terminal extension region like 1-Cys Prx AhpE from *Mycobacterium tuberculosis* previously reported (Li et al., 2005). The *Vv*Prx3 protomer is formed based on a central five-stranded β-sheet (β5-β4-β3-β8-β9). α-Helices α2 and α5 are placed at one side of the central β-sheet, and α4 and a β-hairpin (β1 and β2) is on the other side of the central β-sheet. The strands β4-β3-β8-β9 and the helices α2, α4, and α5 comprise the typical Trx fold (Fig. 5A). At the peripheral region, a structural motif β4-α3-β5 is located in the A-type dimeric interface of

*Vv*Prx3 (C48D/C73S) and *Vv*Prx3 (C73S) (Fig. 5). The C_P Cys48 (or the mutated Asp48) is located at the N-terminus of the long and kinked α2 like other Prxs. The mutated Ser73 is buried in the Trx fold region (Fig. 5A). Structural superposition of the reduced *Vv*Prx3 with human Prx5 (PDB code: 1OC3; sequence identity 52%) revealed a high structural similarity considering an rms difference value of 1.463 between the Cα positions of the matched 247 amino acids (Fig. 6A).

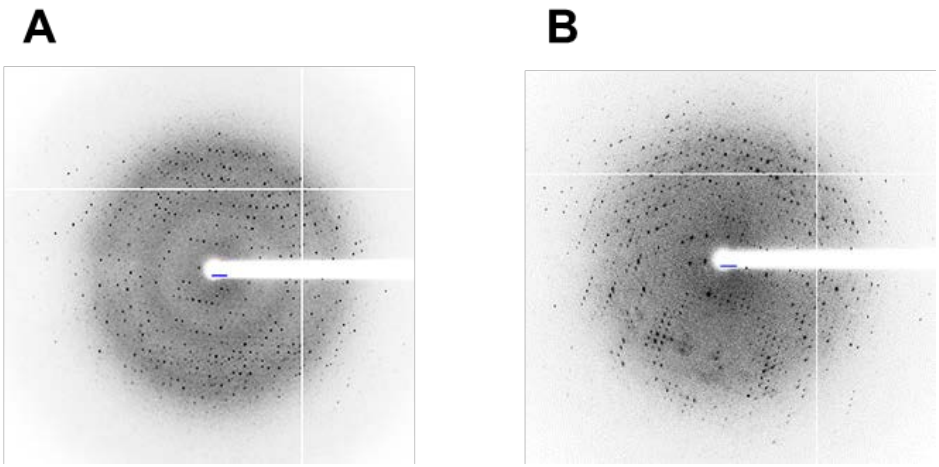

Figure 4. X-ray diffraction images of *Vv*Prx3 (C48D/C73S; A) and *Vv*Prx3 (C73S; B).

Table 1. X-ray statistics for data collection and refinement

	Disulfide-Prx3 (C73S)	**Reduced-Prx3 (C48D/C73S)**	**H_2O_2-binding Prx3 (C48D/C73S)**
Data collection			
Space group	$P2_12_12_1$	$P3_221$	$P1$
Cell dimensions			
a, *b*, *c* (Å)	39.455, 57.443, 124.374	73.871, 73.871, 62.254	75.080, 97.725, 97.492
α, *β*, *γ* (°)	90, 90, 90	90, 90, 120	78.72, 67.34, 67.34
Resolution (Å)	50-1.48 (1.51-1.48)	50 - 1.90 (1.93-1.90)	50 - 1.90 (1.93-1.90)
R_{merge}	0.071 (0.279)	0.058 (0.390)	0.060(0.364)
$I/\sigma I$	25.9 (4.96)	39.0 (4.57)	14.5 (2.07)
Completeness (%)	98.6 (95.1)	99.3 (99.5)	90.0 (82.6)
Redundancy	10 (6)	13.3 (7.1)	3.4 (2.2)
Refinement			
Resolution (Å)	18.93-1.48 (1.52-1.48)	31.99 -1.90 (1.96-1.90)	19.68-1.91 (1.93-1.91)
No. of reflections	47559	14790	137000
R_{work}/R_{free}	0.1806/0.1980	0.2132/0.2582	0.2059/0.2529
No. of total atoms	2568	1197	144384
No. of ligands	0	0	4
No. of water molecules	231	37	484
Wilson B-factor (Å)	23.6	15.7	18.64
R.M.S deviations			
Bond lengths (Å)	0.007	0.007	0.004
Bond angles (°)	1.14	0.87	0.744
Ramachandran plot			
Favored (%)	95.54	94.12	93.54
Allowed (%)	4.46	5.88	6.29
Outliers (%)	0.0	0.0	0.16
Molecules in asymmetric unit	2	1	12
PDB ID	5K2I	5K1G	5K2J

* Values in parentheses are for the highest-resolution shell.

R_{free} value was calculated using a test set size of 9.95%.

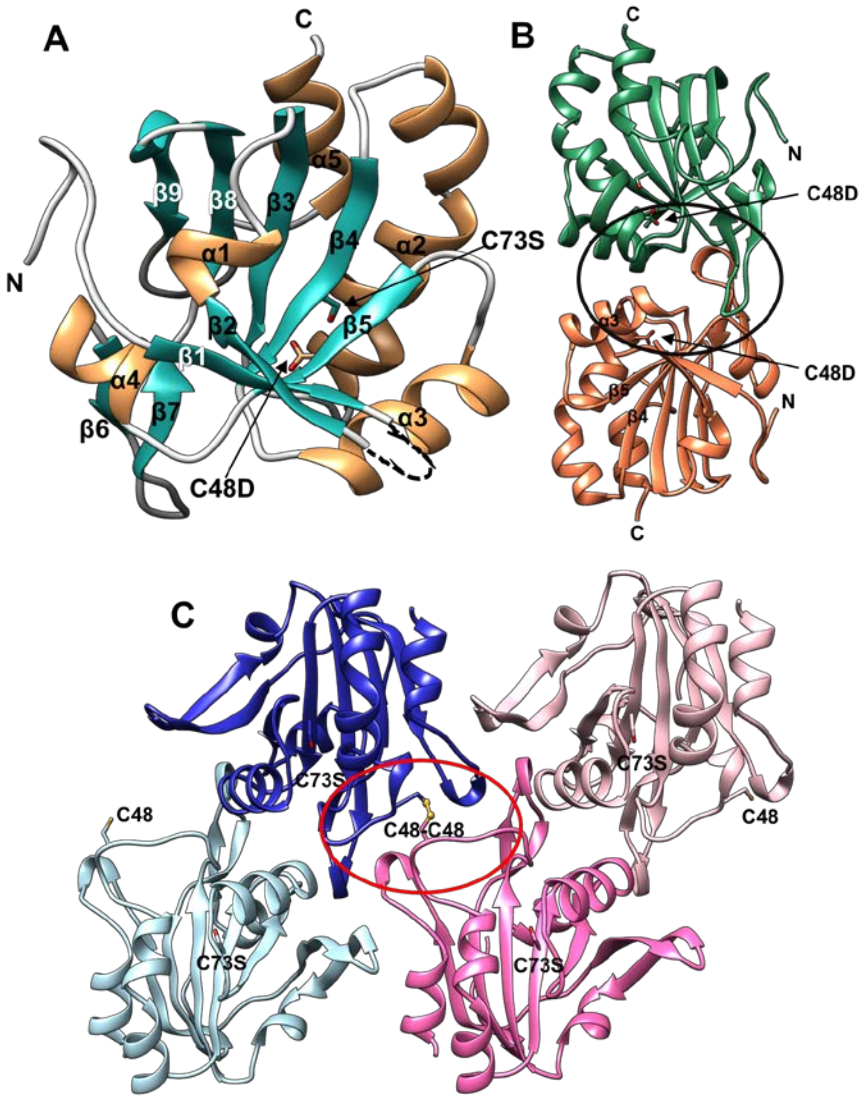

Figure 5. Overall structures *Vv*Prx3 A. Ribbon diagram for a *Vv*Prx3 (C48D/C73S) protomer. A-helices, β-strands, and loops are represented in gold, green, and gray, respectively. The black arrows indicate side chains of the mutated residues, Cys48 and Cys73.

B. The dimeric structure of *Vv*Prx3 (C48D/C73S) in the crystal, formed by the A-type interface. Two protomers were differently colored (green and salmon). The side chains of Cys48 and Cys73 are shown in the ball-and-stick representations. The black arrows indicate side chains of the mutated residue (C48D) and the black circle represents A-type interface of peroxiredoxin.

C. The asymmetric unit of *Vv*Prx3 (C73S) that has intact Cys48 in the disulfide state between the Cys48 residues. Four protomers are drawn in different colors, and the side chains of Cys48 and Ser73 are displayed in the ball-and-stick models. The red circle represents C-type interface of peroxiredoxin.

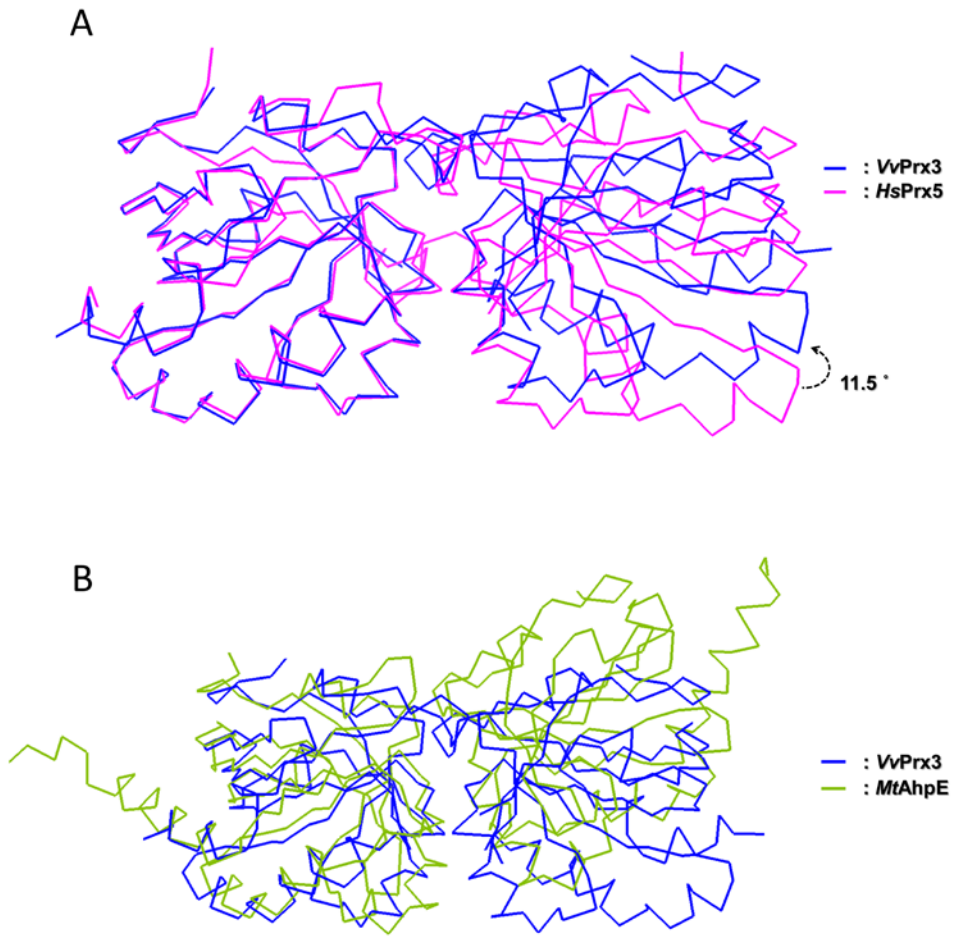

Figure 6. Structural superposition of *Vv*Prx3 with its homologuous proteins. A. The dimeric unit of the *Vv*Prx3 (C48D/C73S) structure at the reduced state (blue) is superposed on *human* Prx5 (magenta; PDB code 1OC3), which is an atypical 2-Cys Prx. B. *Vv*Prx3 (C48D/C73S) (blue) is superposed onto AhpE from *M. tuberculosis* (green; PDB code 1XXU). The black arrow indicated a conformational change between *Vv*Prx3 (C48D/C73S) and *Hs*Prx5.

3.4. Structural comparison between the reduced and disulfide state of *Vv*Prx3

I found that both *Vv*Prx3 structures at the reduced and disulfided states showed a similar dimeric assembly in the crystals, which can be characterized by the A-type dimeric interface like AhpE from *M. tuberculosis* (Fig. 6B) (Li et al., 2005).When the *Vv*Prx3 dimers are superposed on an atypical 2-Cys Prx, human PrxV (Declercq et al., 2001), a slight twist between the protomers was observed (Fig. 6A). In the reduced state, the C_P-containing loop at the active site adopted a "fully-folded" conformation, usually observed in Prx structures in the reduced or the overoxidized states (Fig. 5B) (Karplus and Hall, 2007). The structure of *Vv*Prx3 (C48DC73S) was stabilized by forming salt bridges interacted with Arg78 and Asp121 residues each other (Fig. 7A).

Strikingly, a novel dimeric interface was found in the Prx3 structure in a disulfide state, distinguished from both the A-type and B-type interfaces (Fig. 5A, B). This interface was designated the "C-type" interface since it involves two C_P residues. The C-type interface mainly consists of two C_P-containing loops from adjacent protomers (Fig. 5C, 7B). Hydrophobic interactions were observed in the C-type interface, which appear to further stabilize this dimeric interface. The Phe145 residue in loop β9-α5 of one protomer forms a hydrophobic core with the Phe117 in loop β6-β7, while Pro41 and Pro46 form a hydrophobic core in the loop connecting β3 and α2 of the other molecule (Fig. 7B). Due to disulfide bonds and the hydrophobic interaction, a significant conformational alteration was observed in the active site of helix α2 containing C_P and nearby loops (Fig. 7C). The α-helix was broken and twisted

outward in oxidized forms of *Vv*Prx3, resembling the “locally-unfolded” conformation that was observed in many Prxs at the disulfide state. In addition, loop β9-α5 moved outward from the core while loop β3-α2 became ordered compared to the reduce form of *Vv*Prx3 (Fig. 7C).

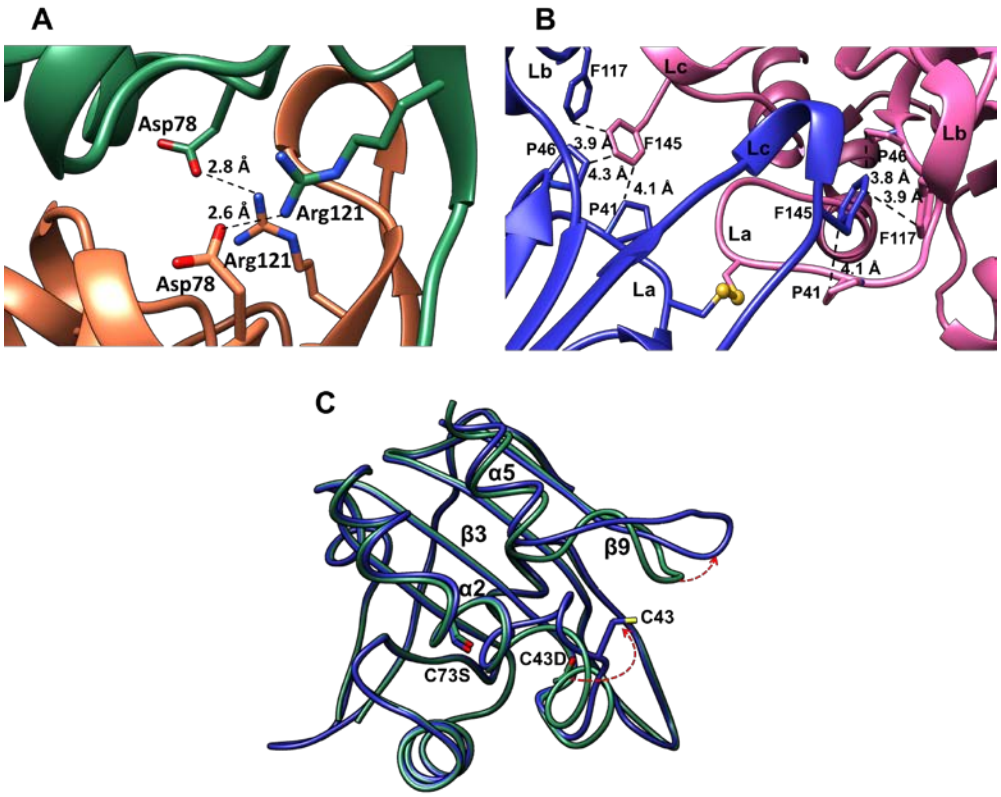

Figure 7. Structural comparison of *Vv*Prx3 between the reduced state and the disulfide state. A. Close-up view of A-type interface of Prx3. The residues which are involved in salt bridge are shown as the balls and sticks with labelling. **B.** Magnified view focusing on the interactions at C-type interface present in the intermolecular disulfide bond between the Cys48 residues. The side-chains involved in hydrophobic core are represented as the balls and sticks with labelling. The loops at this interface are labelled as La, Lb, and Lc indicating the loop connecting β3 and

α2, the loop connecting β6 and β7, and the loop connecting β9 and α5, respectively. The labels from the different protomers are distinguished by ’.

C. Structural superpositions of *Vv*Prx3 of between the reduced form (green) and disulfide form (blue) form of *Vv*Prx3. The red dotted arrows indicate the regions showing the highest conformational changes.

3.5. Peroxide induced intermolecular disulfide formation of *Vv*Prx3

I next tested whether the disulfide bond observed in the crystal is induced by the peroxides or not. H_2O_2 and tertiary butyl hydrogen peroxide (t-BOOH), the known substrates of *Vv*Prx3, were applied to the reduced form of *Vv*Prx3(Beckman and Koppenol, 1996). Reduced *Vv*Prx3 (C73S) protein was incubated with H_2O_2 or t-BOOH and analyzed with SDS-PAGE under non-reducing conditions in order to observe intermolecular disulfide bond formation. While boiling the protein sample for SDS-PAGE, the free cysteine residues seemed to form non-specific disulfide bonds. To avoid these non-specific disulfide bonds, the free thiol-specific alkylating agent iodoacetamide was added to the sample prior to boiling in order to block free cysteines.

As shown in Figs. 8A and B, protein bands indicating dimers of *Vv*Prx3 were generated by treatment with H_2O_2 and t-BOOH on SDS-polyacrylamide gels. The protein bands were down-shifted to a monomeric size when a reducing agent was added to cleave disulfides during the boiling process. These results indicate that two *Vv*Prx3 protomers were linked by an intermolecular disulfide bond between two Cys48 residues. Interestingly, the intensities of the dimeric protein bands decreased at higher concentrations of peroxides. Maximum band intensities were shown at 10 μM of H_2O_2 or t-BOOH (Fig. 8A and B), probably because of overoxidation of C_P at high peroxide concentrations (Kassan et al., 2013). These findings indicate that the intermolecular disulfide bond between C_P residues is induced by the peroxides H_2O_2 and t-BOOH, distinguished from the prevailing mechanisms for 1-Cys Prxs via direct

reduction of C_P-SOH by glutaredoxin (Grx) or GSH (Jeong et al., 2000; Pedrajas et al., 2015).

To determine the speed of dimerization of *Vv*Prx3, the amount of dimeric *Vv*Prx3 was measured using the same SDS-PAGE method with different incubation times. The results showed that dimerization of *Vv*Prx3 occurs within 3 s (Fig. 8C), suggesting that dimerization of *Vv*Prx3 provides a rapid kinetic path to resolving C_P.

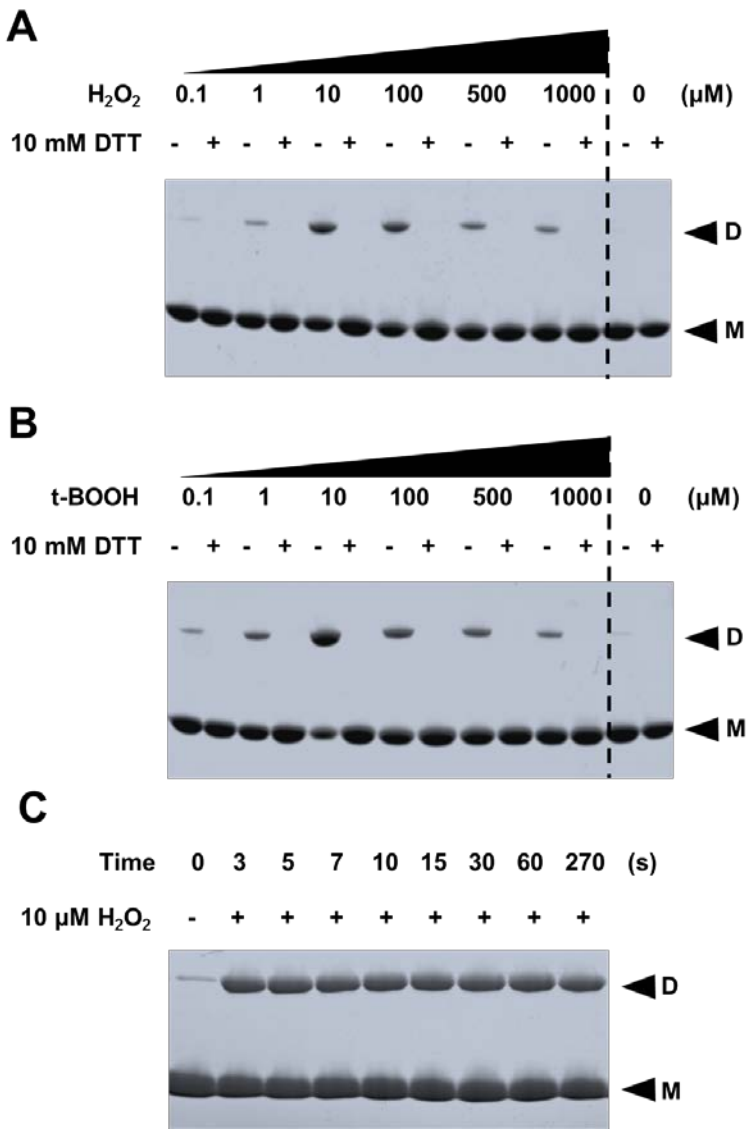
A
H2O2 0.1 1 10 100 500 1000 0 (μM)
10 mM DTT - + - + - + - + - + - + - +
D
M
B
t-BOOH 0.1 1 10 100 500 1000 0 (μM)
10 mM DTT - + - + - + - + - + - + - +
D
M
C
Time 0 3 5 7 10 15 30 60 270 (s)
10 μM H2O2 - + + + + + + + +
D
M

Figure 8. Intermolecular disulfide bond formation of *Vv*Prx3 (C73S) by treatment of peroxides. The proteins were treated with H_2O_2 (**A**) or t-butyl hydrogen peroxide (t-BOOH; **B**) at given concentrations for 30 min, and then stopped by addition of iodoacetamide. The samples were boiled in the presence (+) or in the absence (-) of 10 mM DTT for the SDS-PAGE analysis. **C**. The purified *Vv*Prx3 (C73S) (70 μM) was reacted by 20 μM H_2O_2 for given times, and then analyzed by SDS-PAGE. The protein band of disulfide bond-containing *Vv*Prx3 (*D*) and the bands that lack a disulfide bond (*M*) are indicated.

3.6. The unique redox-dependent oligomerization of *Vv*Prx3

A protein oligomer representing the disulfide state was noted found in *Vv*Prx3 crystals (Fig. 6C). The oligomer is generated in a linear arrangement by alternate connections between the protomers via A-type contact and the C-type contact (Fig. 9A). As observed in Fig. 6C, peroxides induce a disulfide bond between the protomers through the C-type interface. The A-type dimer in the reduced state is further linked by the disulfide bond between the C_P's at the C-type interface, which can lead to the linear oligomer observed in *Vv*Prx3 crystals (Fig. 9A).

To investigate changes in the oligomeric states of *Vv*Prx3 proteins induced by oxidative stress, the oligomeric state and disulfide bond formation of *Vv*Prx3 proteins in the presence/absence of H_2O_2 treatment were analyzed by combining size exclusion chromatography and SDS-PAGE. In these experiments, two Prx variants were applied: C73S and C48D/C73S. To create a disulfide bond between the C_P residues, *Vv*Prx3 (C73S) protein was treated with H_2O_2 before loading on a size exclusion chromatographic column. After the *Vv*Prx3 (C73S) protein was applied to the size exclusion chromatographic column in a buffer devoid of reducing agent, the eluted fractions were analyzed by SDS-PAGE under non-reducing conditions. The elution profile showed a gradually progressing pattern before achieving the dimeric size of *Vv*Prx3, reflecting mixed forms of higher oligomers. Decamer, hexamer, tetramer, or dimer, which were estimated based on the elution volume, were observed (Fig. 9B). Analysis of the fractions with SDS-PAGE under non-reducing conditions enabled examination of the increased amount of dimeric bands without further

oligomeric bands. The higher oligomeric forms of *Vv*Prx3 on the size exclusion chromatographic column were clearly created by non-covalently associated A-type interfaces and disulfide-linked C-type interfaces, as observed in crystals of the *Vv*Prx3 structure in oxidized or disulfide state.

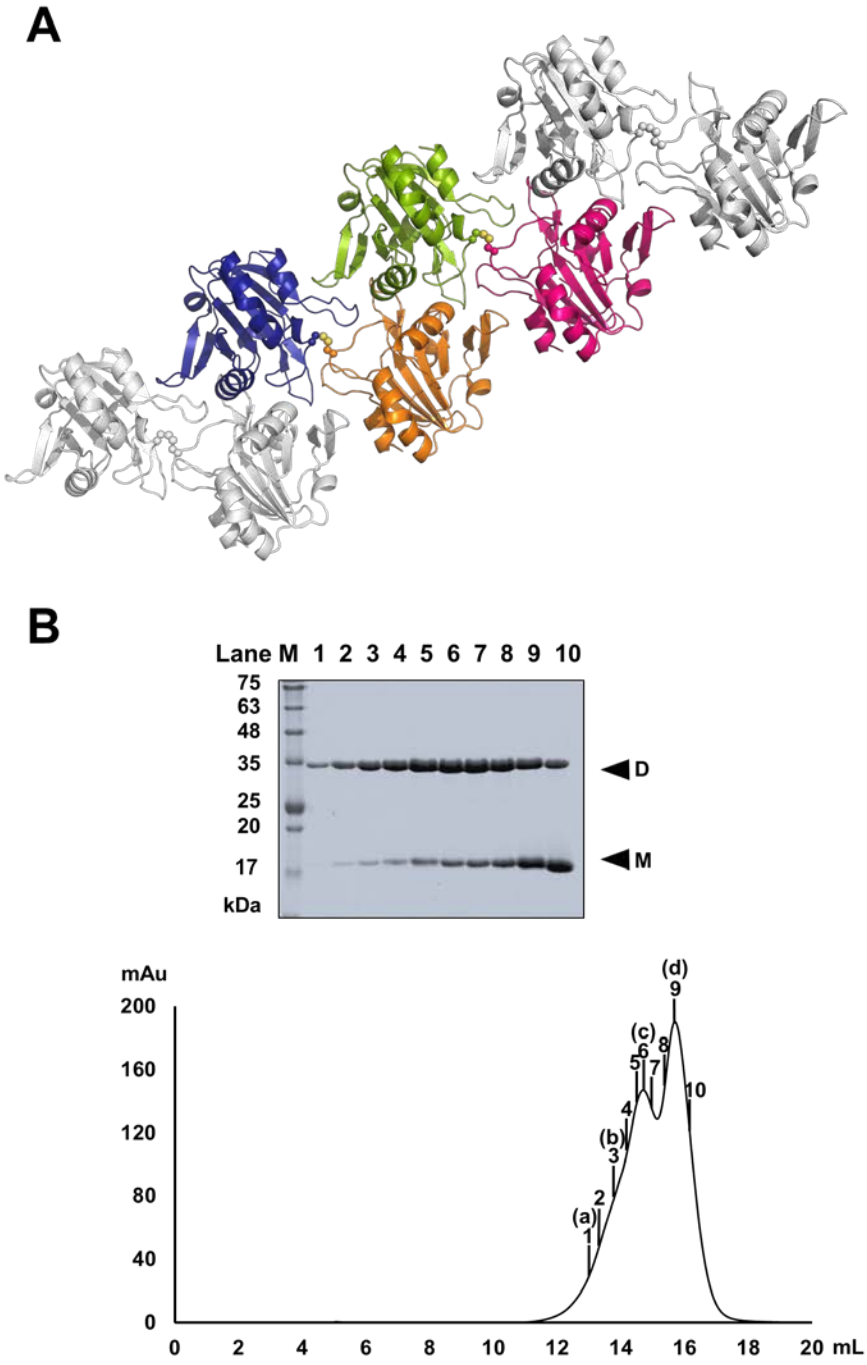
A
B
Lane M 1 2 3 4 5 6 7 8 9 10
75
63
48
35
25
20
17
kDa
D
M
mAu
200
160
120
80
40
0
0 2 4 6 8 10 12 14 16 18 20 mL
(a)
(b)
(c)
(d)
1
2
3
4
5
6
7
8
9
10

Figure 9. Oligomeric assembly observed in *Vv*Prx3 (C73S) structure at the disulfide state in the crystal A. The asymmetric unit is shown in blue, orange, green, or magenta, while adjacent molecules are in gray. Each protomers is connected via disulfide bonds between Cys48's (balls). **B**. Oligomerization states of *Vv*Prx3 in solution were analyzed by using size exclusion chromatography, and the fractions were further analyzed by SDS-PAGE under non-reducing condition. The numbered arrows indicate the derived molecular sizes of *Vv*Prx3 from the standards (Fig 1). (a) decamer (~252 kDa); (b) hexamer (~169 kDa); (c) tetramer (~94 kDa); (d) dimer (~57 kDa). The protein band of disulfide bond-containing *Vv*Prx3 (*D*) and the bands that lack a disulfide bond (*M*) are indicated.

3.7. H_2O_2 binding site

To examine interactions between *Vv*Prx3 and peroxides, the *Vv*Prx3 structure in complex with H_2O_2 was determined. A high concentration (500 μM) of H_2O_2 was incubated with crystals of *Vv*Prx3 (C48D/C73S) in the reduced state, which changed the space group and cell parameters. The crystal structure was determined at 1.9 Å resolution. Electron density maps were well-defined in all 12 protomers in the asymmetric unit, and ovoid-shaped electron density maps indicating H_2O_2 were found near Asp48 and the active site region adopting the fully-folded conformation (Fig 10). The H_2O_2 binding site is fully accessible from the solvent since it is exposed to external medium. The structure is analogous to H_2O_2-bound 2-Cys archaeal Prx, the thioredoxin peroxidase from *Aeropyrum pernix* K1 (Nakamura et al., 2010), in which the corresponding cysteine residue was overoxidized and shares the H_2O_2 binding site. Thus, it is likely that substrate binding near C_P is important in the rapid catalysis of *Vv*Prx3. In Prx structures, only one oxygen atom of H_2O_2 near Cys48 (or Asp48 in my structure) has further interactions with *Vv*Prx3, while the other oxygen atom did not have any interaction with *Vv*Prx3. In OxyR sensing H_2O_2 exclusively, both oxygen atoms in H_2O_2 were extensively involved in polar interaction with OxyR (Jo et al., 2015). This difference in H_2O_2 recognition might result in the different substrate specificities of the two proteins.

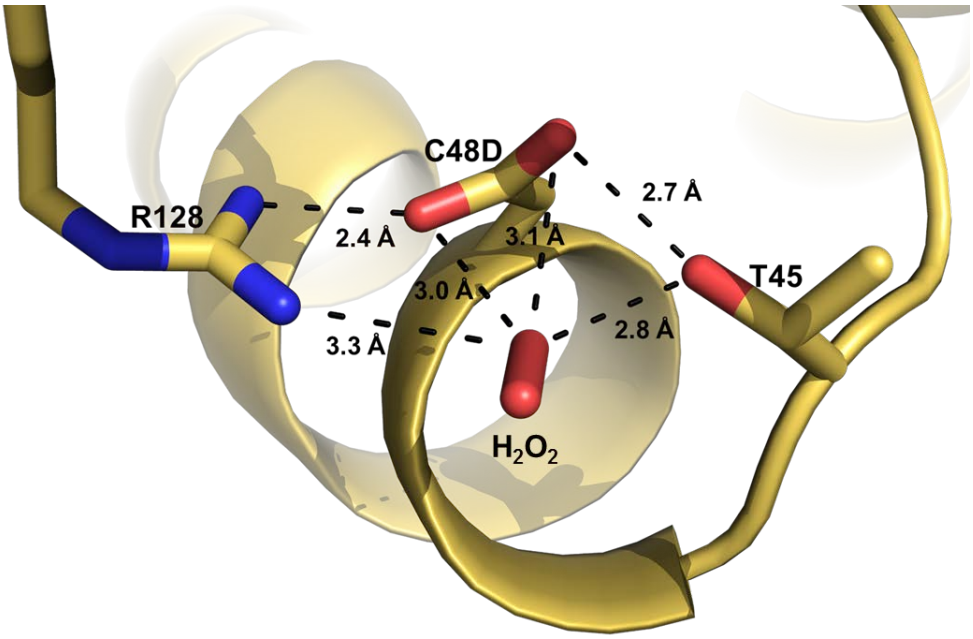

Figure 10. The H_2O_2 binding site in *Vv*Prx3 (C48D/C73S). The bound H_2O_2 and the involved residues are shown in the stick representations in resolution structure at a resolution of 1.9 Å. The broken lines indicate the interactions between the residues and H_2O_2.

3.8. NO induces the intermolecular disulfide

Prxs are also known to scavenge reactive nitrogen stress such as peroxinitrite that is rapidly generated by combining NO and superoxide ion (Fang, 2004; Matsubara et al., 2015). NO is also generated by the human immune system. Since NO and H_2O_2 are similar in size, I hypothesized that NO can induce the disulfide of *Vv*Prx3, like H_2O_2. The relationship between NO stimulation and induction of *Vv*Prx3 in *V. vulnificus* was examined for the first time in this study. NO is an unstable gas that rapidly converts to NO_2 in the presence of oxygen, which makes it difficult to maintain a certain concentration of NO in the reaction mixture. To overcome this problem, this study employed NO-releasing polymeric nanoparticles (NO/PPNPs), which were recently developed to allow sustained release of NO in solution (Nurhasni et al., 2015).

Next, whether or not NO induces disulfide bonds of the *Vv*Prx3 protein was tested. NO/PPNPs were treated with the *Vv*Prx3 protein. Disulfide bond formation of the protein was analyzed by SDS-PAGE and size-exclusion chromatography. Compared to the air-oxidized *Vv*Prx3 protein, a significant amount of protein bands representing the dimer of *Vv*Prx3 increased on the SDS-polyacrylamide gel under non-reducing conditions after treatment of the nanoparticles (NPs) with up to 1 μM NO. The NO concentration in solution is much lower than the effective concentration (~10 μM) of H_2O_2 for *Vv*Prx3 (Fig. 11). Thus, my results suggest that *Vv*Prx3 is capable of scavenging NO through a similar mechanism as with H_2O_2 stress.

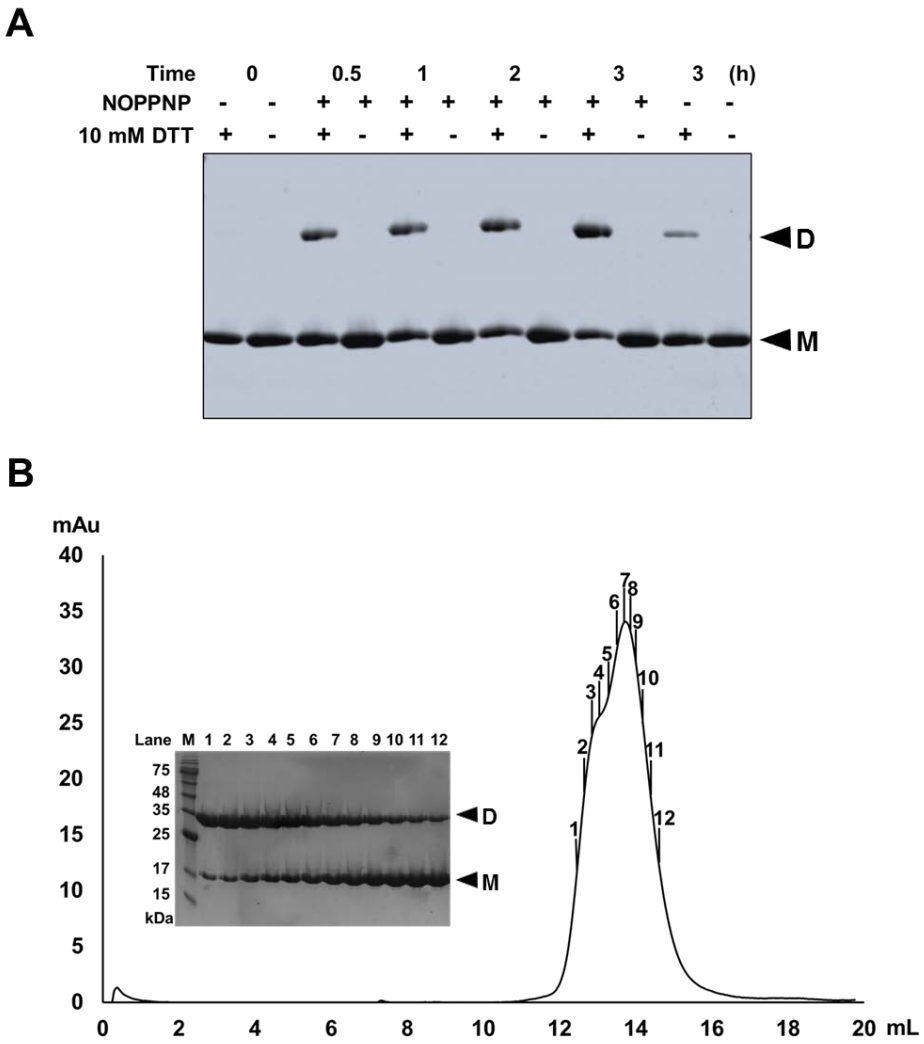

Figure 11. Effect of NO exposure on the *Vv*Prx3 protein. A. *Vv*Prx3 (C73S) was incubated with NO/PPNPs for given times. 3.3 μM of NO is accumulated in the reaction mixture per hour. The reaction was terminated by adding 2.5 mM iodoacetamide to prevent non-specific disulfide bond. Aliquots were taken from the

reaction mixture and then loaded onto SDS-PAGE under reducing condition (DTT; +) or non-reducing condition (DTT; -).

B. Oligomerization states of *Vv*Prx3 in solution by treatment of NO/PPNPs (1 mg). Oligomeric states were analyzed by using size exclusion chromatography, combined with SDS-PAGE under non-reducing condition. The protein band of disulfide bond-containing *Vv*Prx3 (*D*) and the bands that lack a disulfide bond (*M*) are indicated.

3.9. *Vv*Prx3 are reduced dependent on Grx3 rather than GSH.

The *Vv*Prx3 at the disulfide state should be rapidly reduced to act on another substrate molecule. Grx3, together with GSH, was known as a key protein for the function of *Vv*Prx3 in *V. vulnificus* (Pedrajas et al., 2010). To figure out how Grx3 and GSH are involved in reducing the disulfide of *Vv*Prx3, I tested if the reduced forms of 15 μM Grx3 or 30 μM GSH can cleave the disulfide of *Vv*Prx3. As shown in Fig. 12A, the Grx3 protein mediated the conversion of the dimeric form to the monomeric form depending on the incubation time. However, incubation with GSH at 30 μM failed to reduction of the disulfide of *Vv*Prx3 (Fig. 12B). However, a higher concentration (100 μM) GSH were able to partly cleave the disulfide of the protein (data not shown). My findings indicate that the disulfide of *Vv*Prx3 between C_P's is more efficiently reduced by Grx3 than GSH.

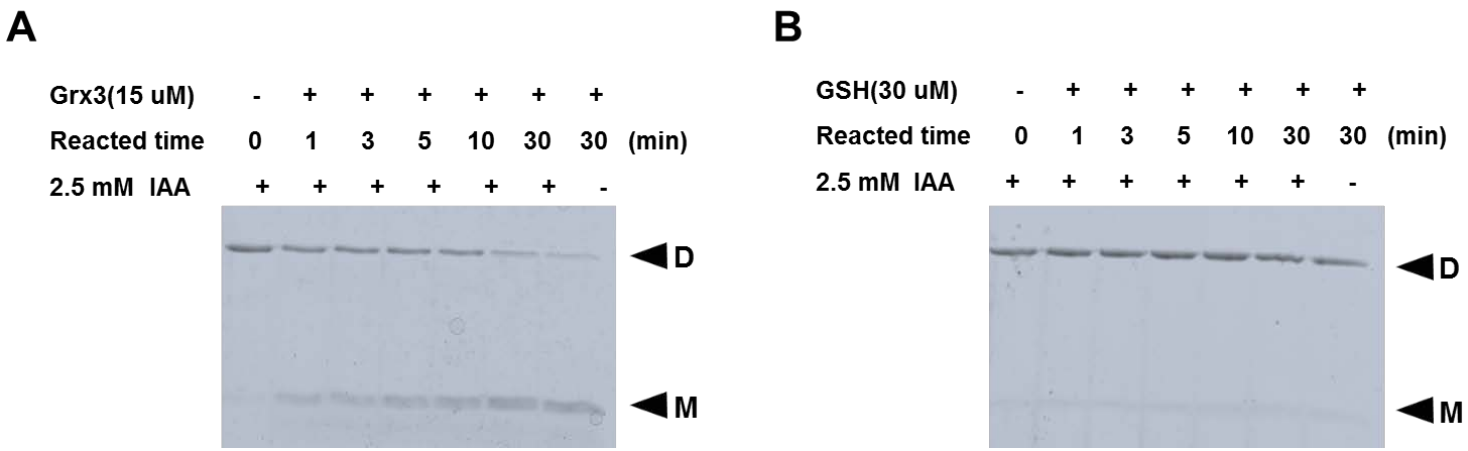

Figure 12. *Vv*Prx3 are reduced dependent on the Grx3 and GSH. The *Vv*Prx3 protein with the intermolecular disulfide bond was incubated with Grx3 (15 μM; A) or GSH (30 μM; B) for given times, and then was separated by SDS-PAGE under non-reducing conditions after adding 2.5 mM IAA to stop the reaction.

IV. DISCUSSION

The crystal structures of *Vv*Prx3, a bacterial 1-Cys Prx, were determined at different redox states in this study. The H_2O_2 binding site near the C_P residue was also shown. Although structural and sequence similarities with 1-Cys Prx AhpE from *M. tuberculosis* were identified, especially in dimeric assembly with the A-type interface, my structures provide some unexpected and important insights into the function and molecular mechanism of 1-Cys Prxs. One striking feature of *Vv*Prx3 in the oxidized state is a novel dimeric interface, designated the C-type interface in this study. Protein-protein interaction at the C-type interface was induced by both NO and peroxides. Due to the oxidation-dependent C-type interface, *Vv*Prx3 formed a higher-order linear oligomer in response to peroxides or NO. This linear oligomeric structure is distinct from the circular decameric assembly of typical 2-Cys Prxs, which is generated by alternate A- and B-type interfaces and is favored in the reduced and overoxidized states (Schroder et al., 2000; Wood et al., 2003b). Since the oligomer of *Vv*Prx3 is generated only in the oxidized state, the redox-dependent oligomerization of *Vv*Prx3 is opposite that of typical 2-Cys Prxs.

According to prevailing mechanisms, 1-Cys Prxs is itself oxidized to C_P-SOH through attack of the substrate peroxide. Then, C_P-SOH is reduced by the reductase Grx or GSH. In this study, the results of *Vv*Prx3 are evidence to support a different pathway for the reduction of C_P-SOH in 1-Cys Prxs. In this pathway, the catalytic

cysteine residue (C_P) in 1-Cys Prx plays a dual role in the catalytic cycle. Not all *Vv*Prx3 proteins are simultaneously oxidized by H_2O_2. Thus, remaining or unreacted *Vv*Prx3 could act on other *Vv*Prx3 with C_P-SOH. The C_P-SOH can be reduced and resolved by free C_P in a different dimer of *Vv*Prx3, in which the free C_P acted as a C_R. The complemental structural features at the C-type interface provide specific interactions with *Vv*Prx3 proteins, facilitating prompt formation of a disulfide bond between C_P-SOH and the free C_P of *Vv*Prx3 proteins (Fig. 6C). This reaction could also occur successively, leading to formation of the linear oligomers observed in the crystal structure (Fig. 9A). Finally, cellular GSH or Grx that is reduced by GSH reduces the disulfide bond in the oligomer. NO is held in the H_2O_2 binding site of the *Vv*Prx3 active site to be readily attacked by C_P. The free C_P from another *Vv*Prx3 resolves the resulting nitrosylated cysteine (C_P-NO), as depicted in Fig. 13.

Many different members are present in 1-Cys Prxs. Of these, 1-Cys Prxs from yeast are relatively well characterized. As in *Vv*Prx3, the intermolecular disulfide bond between C_P was observed in yeast 1-Cys Prx, resulting in oligomeric assembly. However, no structural studies of this protein have been reported. I speculate that yeast 1-Cys Prx might share a catalytic cycle with *Vv*Prx3, although further studies are required to elucidate its mechanisms.

Increasing attention has been given to NO-mediated reactions of host immune systems (Spahich et al., 2016). Herein, I performed experiments with proteins and live bacteria using NO/PPNPs. A large amount of NO is synthesized in macrophages or epithelial cells stimulated by pathogens or substances secreted from pathogens

(Fang and Vazquez-Torres, 2002; Torraca et al., 2014). The pathogenic bacterium *V. vulnificus* should defend against NO stress to increase survival in the host environment. A previous study showed that *Vv*Prx3 is important in the pathogenicity of *V. vulnificus* in mice (Lim et al., 2014). These findings suggest that *Vv*Prx3 is important in bacterial survival in NO-challenged environments and might account for *Vv*Prx3 involvement in pathogenicity in the host.

Diverse types of peroxiredoxins exist in nature and play different roles in the scavenging of toxic radicals. I proposed the molecular mechanism for bacterial 1-Cys Prx and a new role in scavenging NO in this study, which can in part account for the pathogenesis of *V. vulnificus*. The structure and mechanism of Prx3 would help develop novel inhibitors which can control the devastating food-borne pathogen *V. vulnificus* can be developed. My findings also expand the understanding of the molecular mechanism of pathogenic bacteria survival in the host environment by scavenging diverse oxidative stresses.

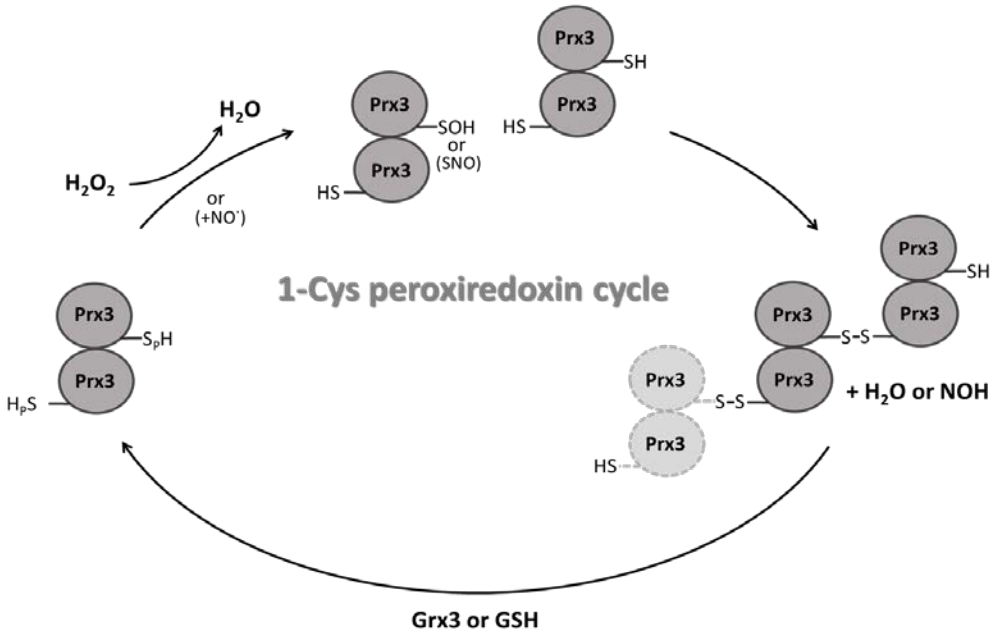

Figure 13. A proposed catalytic cycle of 1-Cys Prx3.

Each Prx3 polypeptide is represented by gray circles with their peroxidatic Cys48 highlighted by the different redox states: sulfhydryl– SH, sulfenic–SOH, nitrosothiol–SNO, and disulfide–S-S-. Potential conformations of additional dimer indicated by bright gray oval.

V. REFERENCES

Afonine, P.V., Grosse-Kunstleve, R.W., Echols, N., Headd, J.J., Moriarty, N.W., Mustyakimov, M., Terwilliger, T.C., Urzhumtsev, A., Zwart, P.H., and Adams, P.D. (2012). Towards automated crystallographic structure refinement with phenix.refine. *Acta crystallographica Section D, Biological crystallography 68*, 352-367.

Beckman, J.S., Beckman, T.W., Chen, J., Marshall, P.A., and Freeman, B.A. (1990). Apparent hydroxyl radical production by peroxynitrite: implications for endothelial injury from nitric oxide and superoxide. *Proceedings of the National Academy of Sciences of the United States of America 87*, 1620-1624.

Beckman, J.S., and Koppenol, W.H. (1996). Nitric oxide, superoxide, and peroxynitrite: the good, the bad, and ugly. *The American journal of physiology 271*, C1424-1437.

Cabiscol, E., Tamarit, J., and Ros, J. (2000). Oxidative stress in bacteria and protein damage by reactive oxygen species. *International microbiology : the official journal of the Spanish Society for Microbiology 3*, 3-8.

Declercq, J.P., Evrard, C., Clippe, A., Stricht, D.V., Bernard, A., and Knoops, B. (2001). Crystal structure of human peroxiredoxin 5, a novel type of mammalian peroxiredoxin at 1.5 A resolution. *Journal of molecular biology 311*, 751-759.

Emsley, P., Lohkamp, B., Scott, W.G., and Cowtan, K. (2010). Features and development of Coot. *Acta crystallographica Section D, Biological crystallography 66*, 486-501.

Evrard, C., Capron, A., Marchand, C., Clippe, A., Wattiez, R., Soumillion, P., Knoops, B., and Declercq, J.P. (2004). Crystal structure of a dimeric oxidized form of human peroxiredoxin 5. *Journal of molecular biology 337*, 1079-1090.

Fang, F.C. (2004). Antimicrobial reactive oxygen and nitrogen species: concepts and controversies. *Nature reviews Microbiology 2*, 820-832.

Fang, F.C., and Vazquez-Torres, A. (2002). Nitric oxide production by human macrophages: there's NO doubt about it. *American journal of physiology Lung cellular and molecular physiology 282*, L941-943.

Hall, A., Nelson, K., Poole, L.B., and Karplus, P.A. (2011). Structure-based Insights into the Catalytic Power and Conformational Dexterity of Peroxiredoxins. *Antioxidants & redox signaling 15*, 795-815.

Hirotsu, S., Abe, Y., Okada, K., Nagahara, N., Hori, H., Nishino, T., and Hakoshima, T. (1999). Crystal structure of a multifunctional 2-Cys peroxiredoxin heme-binding protein 23 kDa/proliferation-associated gene product. *Proceedings of the National Academy of Sciences of the United States of America 96*, 12333-12338.

Ho, S.N., Hunt, H.D., Horton, R.M., Pullen, J.K., and Pease, L.R. (1989). Site-directed mutagenesis by overlap extension using the polymerase chain reaction. *Gene 77*, 51-59.

Huaxia, Y., Wang, F., Yan, Y., Liu, F., Wang, H., Guo, X., and Xu, B. (2015). A novel 1-Cys thioredoxin peroxidase gene in *Apis cerana cerana*: characterization of AccTpx4 and its role in oxidative stresses. *Cell stress & chaperones 20*, 663-672.

Hyduke, D.R., Jarboe, L.R., Tran, L.M., Chou, K.J., and Liao, J.C. (2007). Integrated network analysis identifies nitric oxide response networks and dihydroxyacid dehydratase as a crucial target in *Escherichia coli*. *Proceedings of the National Academy of Sciences of the United States of America 104*, 8484-8489.

Jeong, W., Cha, M.K., and Kim, I.H. (2000). Thioredoxin-dependent hydroperoxide peroxidase activity of bacterioferritin comigratory protein (BCP) as a new member of the thiol-specific antioxidant protein (TSA)/Alkyl hydroperoxide peroxidase C (AhpC) family. *The Journal of biological chemistry 275*, 2924-2930.

Jiao, L., Kim, J.S., Song, W.S., Yoon, B.Y., Lee, K., and Ha, N.C. (2013). Crystal structure of the periplasmic disulfide-bond isomerase DsbC from *Salmonella enterica serovar Typhimurium* and the mechanistic implications. *Journal of structural biology 183*, 1-10.

Jo, I., Chung, I.Y., Bae, H.W., Kim, J.S., Song, S., Cho, Y.H., and Ha, N.C. (2015). Structural details of the OxyR peroxide-sensing mechanism. *Proceedings of the National Academy of Sciences of the United States of America 112*, 6443-6448.

Karplus, P.A., and Hall, A. (2007). Structural survey of the peroxiredoxins. *Sub-cellular biochemistry 44*, 41-60.

Kassan, M., Lasker, G.F., Sikka, S.C., Mandava, S.H., Gokce, A., Matrougui, K., Hellstrom, W.J., Kadowitz, P.J., and Serefoglu, E.C. (2013). Chronic escitalopram treatment induces erectile dysfunction by decreasing nitric oxide bioavailability mediated by increased nicotinamide adenine dinucleotide phosphate oxidase activity and reactive oxygen species production. *Urology 82*, 1188 e1181-1187.

Knoops, B., Goemaere, J., Van der Eecken, V., and Declercq, J.P. (2011). Peroxiredoxin 5: structure, mechanism, and function of the mammalian atypical 2-Cys peroxiredoxin. *Antioxidants & redox signaling 15*, 817-829.

Lee, S., Jia, B., Liu, J., Pham, B.P., Kwak, J.M., Xuan, Y.H., and Cheong, G.W. (2015). A 1-Cys Peroxiredoxin from a *Thermophilic Archaeon Moonlights* as a Molecular Chaperone to Protect Protein and DNA against Stress-Induced Damage. *PloS one 10*, e0125325.

Li, S., Peterson, N.A., Kim, M.Y., Kim, C.Y., Hung, L.W., Yu, M., Lekin, T., Segelke, B.W., Lott, J.S., and Baker, E.N. (2005). Crystal Structure of

AhpE from *Mycobacterium tuberculosis*, a 1-Cys peroxiredoxin. *Journal of molecular biology 346,* 1035-1046.

Lim, J.G., Bang, Y.J., and Choi, S.H. (2014). Characterization of the *Vibrio vulnificus* 1-Cys peroxiredoxin Prx3 and regulation of its expression by the Fe-S cluster regulator IscR in response to oxidative stress and iron starvation. *The Journal of biological chemistry 289,* 36263-36274.

Matsubara, K., Higaki, T., Matsubara, Y., and Nawa, A. (2015). Nitric oxide and reactive oxygen species in the pathogenesis of *preeclampsia*. *International journal of molecular sciences 16,* 4600-4614.

Murray, H.W., and Nathan, C.F. (1999). Macrophage microbicidal mechanisms in vivo: reactive nitrogen versus oxygen intermediates in the killing of intracellular visceral *Leishmania donovani*. *The Journal of experimental medicine 189,* 741-746.

Nakamura, T., Kado, Y., Yamaguchi, T., Matsumura, H., Ishikawa, K., and Inoue, T. (2010). Crystal structure of peroxiredoxin from *Aeropyrum pernix* K1 complexed with its substrate, hydrogen peroxide. *Journal of biochemistry 147,* 109-115.

Nurhasni, H., Cao, J., Choi, M., Kim, I., Lee, B.L., Jung, Y., and Yoo, J.W. (2015). Nitric oxide-releasing poly(lactic-co-glycolic acid)-polyethylenimine nanoparticles for prolonged nitric oxide release, antibacterial efficacy, and in vivo wound healing activity. *International journal of nanomedicine 10,* 3065-3080.

Otwinowski, Z., and Minor, W. (1997). Processing of X-ray diffraction data collected in oscillation mode. *Method Enzymol 276*, 307-326.

Parsonage, D., Youngblood, D.S., Sarma, G.N., Wood, Z.A., Karplus, P.A., and Poole, L.B. (2005). Analysis of the link between enzymatic activity and oligomeric state in AhpC, a bacterial peroxiredoxin. *Biochemistry 44*, 10583-10592.

Pedrajas, J.R., McDonagh, B., Hernandez-Torres, F., Miranda-Vizuete, A., Gonzalez-Ojeda, R., Martinez-Galisteo, E., Padilla, C.A., and Barcena, J.A. (2015). Glutathione Is the Resolving Thiol for Thioredoxin Peroxidase Activity of 1-Cys Peroxiredoxin Without Being Consumed During the Catalytic Cycle. *Antioxidants & redox signaling*.

Pedrajas, J.R., Padilla, C.A., McDonagh, B., and Barcena, J.A. (2010). Glutaredoxin participates in the reduction of peroxides by the mitochondrial 1-CYS peroxiredoxin in *Saccharomyces cerevisiae*. *Antioxidants & redox signaling 13*, 249-258.

Randall, L., Manta, B., Nelson, K.J., Santos, J., Poole, L.B., and Denicola, A. (2016). Structural changes upon peroxynitrite-mediated nitration of peroxiredoxin 2; nitrated Prx2 resembles its disulfide-oxidized form. *Archives of biochemistry and biophysics 590*, 101-108.

Rhee, S.G., Jeong, W., Chang, T.S., and Woo, H.A. (2007). Sulfiredoxin, the cysteine sulfinic acid reductase specific to 2-Cys peroxiredoxin: its

discovery, mechanism of action, and biological significance. *Kidney international Supplement*, S3-8.

Schroder, E., Littlechild, J.A., Lebedev, A.A., Errington, N., Vagin, A.A., and Isupov, M.N. (2000). Crystal structure of decameric 2-Cys peroxiredoxin from human erythrocytes at 1.7 A resolution. *Structure 8*, 605-615.

Spahich, N.A., Vitko, N.P., Thurlow, L.R., Temple, B., and Richardson, A.R. (2016). *Staphylococcus aureus* lactate- and malate-quinone oxidoreductases contribute to nitric oxide resistance and virulence. *Molecular microbiology.*

Torraca, V., Masud, S., Spaink, H.P., and Meijer, A.H. (2014). Macrophage-pathogen interactions in infectious diseases: new therapeutic insights from the zebrafish host model. *Disease models & mechanisms 7*, 785-797.

Winn, M.D., Ballard, C.C., Cowtan, K.D., Dodson, E.J., Emsley, P., Evans, P.R., Keegan, R.M., Krissinel, E.B., Leslie, A.G., McCoy, A., *et al.* (2011). Overview of the CCP4 suite and current developments. *Acta crystallographica Section D, Biological crystallography 67*, 235-242.

Wood, Z.A., Poole, L.B., Hantgan, R.R., and Karplus, P.A. (2002). Dimers to doughnuts: redox-sensitive oligomerization of 2-cysteine peroxiredoxins. *Biochemistry 41*, 5493-5504.

Wood, Z.A., Poole, L.B., and Karplus, P.A. (2003a). Peroxiredoxin evolution and the regulation of hydrogen peroxide signaling. *Science 300*, 650-653.

Wood, Z.A., Schroder, E., Robin Harris, J., and Poole, L.B. (2003b). Structure, mechanism and regulation of peroxiredoxins. *Trends in biochemical sciences 28*, 32-40.

VI. 국문초록

패혈증 비브리오는 기회 감염균으로 오염된 해산물을 날 것으로 섭취하거나, 상처가 난 신체 부위를 통해 균이 감염되면 심각한 패혈증을 유발 하는 병원균이다. 특히 만성 간 질환이나 당뇨를 가진 환자, 또는 면역력이 약화된 사람이 감염되는 경우에는 치명적인 패혈증이 발병하여 질환이 없는 건강한 사람에 비하여 사망할 확률이 높게 증가한다. 숙주세포가 병원균에 감염되면 숙주세포의 면역 반응에 의해 활성산소종(ROS)와 활성질소종(RNS)이 분비된다. 이러한 환경에서 살아남기 위해 병원균은 숙주세포의 면역반응에 대한 방어 시스템을 가지는 방향으로 진화해왔다. 패혈증 비브리오균에서 Peroxiredoxin 은 활성산소종(ROS)을 방어하는 단백질로, Cysteine 을 기반으로 작용한다. 최근 연구에 따르면 패혈증 비브리오균에서 OxyR 에 의해 발현이 조절되는 peroxiredoxin 들과는 다르게 전사 조절자인 IscR 에 의해 발현이 조절되는 1-Cys Peroxiredoxin(Prx3)가 중요한 독성인자로 작용한다는 보고가 있었다. 본 연구에서는 Prx3 의 작용기전을 알아보기 위해 산화 그리고 환원된 상태의 구조를 각각 1.5 Å 과 1.9 Å 해상도로 규명하였다. 산화된 상태의 구조에서는 Peroxiredoxin 에서 일반적으로 관찰되는 A 형 인터페이스와 더불어 두 개의 단백질이 서로 이황화결합을

이루고 있는 새로운 인터페이스를 발견하였다. 이 새로운 인터페이스를 Cysteine 에 의해 형성된 인터페이스라는 의미로 C 형 인터페이스라 명명하였다. 단백질 결정 구조를 통해 관찰한 C 형 인터페이스는 Prx3 의 리간드로 알려져 있는 과산화수소와 삼차부틸히드로과산화물(t-BOOH) 그리고 숙주세포의 면역반응에 의해 유도되는 주요 물질인 일산화질소에 의해서도 형성되었다. 또한 peroxiredoxin 의 재순환(recycling)단계에서 Grx3 가 높은 효율로 이황화결합을 끊어주는 것을 SDS-PAGE 분석을 통해 확인하였다. 종합하면 1-Cys peroxiredoxin 이 일산화질소를 제어할 수 있다는 새로운 기능과 구조 분석을 통해 모색한 분자적인 작용기전을 제시하여 패혈증 비브리오균의 방어 기전에 대하여 규명할 수 있었다. 이를 통해 패혈증 비브리오균이 인간에게 감염되었을 때 Prx3 가 인간의 면역반응에 의해 발생하는 활성산소종과 활성질소종을 제어하여 패혈증 비브리오균이 체내에 생존할 것으로 판단된다. 나아가 본 연구를 통해 구조를 기반으로 Prx3 의 기능을 제어하는 저해제를 개발하여 패혈증 비브리오에 의한 식중독을 예방하는 식품 살균제의 발전에 기여할 수 있을 것이다.

주요어: 패혈증 비브리오균, 1-Cys Prx, 과산화수소, 일산화질소

학번: 2014-22933